EAST EUROPEAN JOURNAL OF PHYSICS. 3. 665-680 (2026)
DOI: 10.26565/2312-4334-2026-3-63 ISSN 2312-4334

# DFT INSIGHTS INTO STRUCTURAL, OPTOELECTRONIC AND THERMODYNAMIC CHARACTERISTICS OF CHALCOPYRITE $AgAl(S_{1-x}Se_x)_2$

**Nabil Beloufa[1,2], Mohammed Ouled Ali[2,3], Hamza Rekab-Djabri[2,4], D. Belfennache[5], R. Yekhlef[5], Hamad M. Adress Hasan[6], Hanan F. Emrayed[6], Haneebal Saeid Khatab[7], Ghada M. Salem[8]**

[1]*Hydrometeorological Institute for Training and Research IHFR, IbnouRochd.Bp 7019, Oran Algeria*
[2]*Laboratory of Micro and Nanophysics (LaMiN), National Polytechnic School Oran, ENPO-MA, BP 1523, El M'Naouer, 31000, Oran, Algeria*
[3]*Faculty of Matter Sciences, Mathematics and Computer Sciences, University of Ahmed Draia, Adrar, Algeria*
[4]*Faculty of Nature and Life Sciences and Earth Sciences, AkliMohand-Oulhadj University, 10000, Bouira, Algeria*
[5]*Research Center in Industrial Technologies CRTI, P.O. Box 64, Cheraga, 16014 Algiers, Algeria*
[6]*Chemistry Department, Faculty of Science, Omar Al-Mukhtar University, Libya*
[7]*Chemistry Department, Faculty of Education, Al-Marj, University of Benghazi, Libya*
[8]*Libyan Authority for Scientific Research, Tripoli, Libya*
**Correspondence Author e-mail: belfennachedjamel@gmail.com*
Received June 19, 2026; revised August 8, 2026; accepted August 12, 2026

In this study, we have investigated the structural, optoelectronic, and thermodynamic properties of the quaternary compound $AgAl(S_xSe_{1-x})_2$. This research employed the FP-LAPW method implemented in the Wien2k program and integrated into the density functional theory (DFT) framework. The generalized gradient approximation (WC-GGA) is used to handle the exchange and correlation potential. We have studied the impact of composition on the formation strength, apparent elastic modulus, and volume of the crystal lattice. According to the data collected, no deviation is noted in the compressibility modulus compared to the LCD law, nor in the lattice constant compared to Vegard's law. The approach of Zunger and his collaborators was used to determine the microscopic source of spatial curvature. Compared to previous theoretical research, the band gap values derived from band structure calculations based on the modified Becke-Johnson (mBJ) potential approximation show notable improvements and align much better with experimental results for ternary compounds. The optical properties indicate that the static dielectric constant $\varepsilon_1(0)$ increases with an increase in concentration x, while the optical gap energy decreases simultaneously; meanwhile, the dielectric function exhibits significant anisotropy in the zz direction. The study of the effects of thermal energy on certain macroscopic characteristics was carried out using Debye's quasi-harmonic model. Nevertheless, the alloys examined showed stability at intermediate temperatures ranging from 0 to 800 K.
**Keywords:** *$AgAl(S_xSe_{1-x})_2$; FP-LAPW; WC-GGA; mBJ; Vegard law; Debye's quasi-harmonic*

## 1. INTRODUCTION

Ternary semiconductor materials, valued for their distinct structures and physical properties, are attracting increased interest within the scientific research community because of their well-localized band gap, which makes them suitable for a variety of electronic applications [1-3]. These crystalline compounds belonging to the ternary systems I-III–$VI_2$ and I–IV–$VI_2$ are particularly significant [4,5]. Under standard thermodynamic conditions, these materials have a crystal structure similar to that of chalcopyrite. [6]. The initial study of chalcopyrite compounds was conducted because of their low conductivity [7]. They offer a multitude of applications [8], including in photovoltaic detectors, optical modulators, optical filters [9], and light-emitting diodes (LEDs) [10]. In addition, these materials can be deliberately doped with various impurities, including magnetic elements, which promotes the emergence of new categories of materials such as dispersed magnetic semiconductors (DMS) [11]. These doped chalcopyrite compounds have considerable potential for emerging technologies in the fields of spintronics [12], optoelectronic devices [13], and advanced photovoltaic systems [14].

Among the advantages of chalcopyrite semiconductors are that they are manufactured in thin layers, either p-type or n-type [15], enabling low-cost production of a variety of homo junction and hetero junction components [16]. They are direct-band gap semiconductors, a factor that minimizes the diffusion length of minority charge carriers [17]. and have a band gap energy within the optimal range for converting solar energy into electrical energy at the Earth's surface (AM1.5) [18].

The first researchers to use density functional theory (DFT) to determine the electronic structures and optical characteristics of a variety of Cu-III-$VI_2$ chalcopyrite ternary materials were Jaffe and Zunger [19]. Several studies [20-23] have been conducted on the electronic and electro-optical characteristics of $AgAlX_2$ (X = S, Se, Te) at atmospheric

***Cite as:*** N. Beloufa, M.O. Ali, H. Rekab-Djabri, D. Belfennache, R. Yekhlef, H.M.A. Hasan, H.F. Emrayed, H.S. Khatab, G.M. Salem, East Eur. J. Phys. 3, 665 (2026), https://doi.org/10.26565/2312-4334-2026-3-63

pressure, which crystallize according to the tetragonal structure of space group $I\bar{4}2d$ and exhibit a direct band gap. In-depth study of these chalcopyrite semiconductors under high pressure has generated considerable scientific interest due to their phase change behavior and unique electronic characteristics. The ternary chalcopyrites $AgAlS_2$ and $AgAlSe_2$ Crystallize in a tetragonal structure of space group I-42d (No. 122), which is typical of chalcopyrite-type semiconductors. The lattice parameters reported for $AgAlS_2$ are a = 5.48 Å and c = 10.93 Å, while those for $AgAlSe_2$ are slightly larger due to the substitution of sulfur by selenium, with a = 5.71 Å and c = 11.37 Å [24, 25]. These materials have a derived structure of the sphalerite type, in which $Ag^+$ and $Al^{3+}$cations occupy distinct tetrahedral sites [19]. At 300°C and a pressure of 25 kbar (≈2.5 GPa), the $AgAlS_2$ chalcopyrite phase transitions to a high-pressure phase known as $AgAlS_2$–II, with trigonal P3ml symmetry and crystal parameters a = 3.50 Å, c = 6.84 Å, and Z = 1 [26]. In their very first research, Honeyman and Wilkinson [27] utilized iodine vapor transport to expand single crystals of $CuGaS_2$, $CuAlTe_2$, $AgGaS_2$, $AgAlS_2$, and $AgAlSe_2$ in order to measure the band gap and refractive index of the systems. Previous research has mainly focused on the use of $AgInS_2$ for photo catalysis and luminescence emission in silver-based I-III-$VI_2$ compounds [28]. Previous experiments carried out with similar compounds such as $AgAlSe_2$ and $AgAlS_2$ have shown that chalcopyrite materials are capable of structural phase transitions [29]. Among the chalcopyrite materials studied in this work are the compounds $AgAl(S_xSe_{1-x})_2$ with x=0, 0.25, 0.5, and 1, which belong to the I-III-$VI_2$ groups.

The band gap is a critical parameter for electronic performance [30]. This is because an increase in sulfur content (x) causes the gap to widen, typically from around 1.9 eV for $AgAlSe_2$ to nearly 2.6 eV for $AgAlS_2$ [26]. In addition, these materials have good chemical stability and favorable electronic transport properties, making it possible to integrate them into thin-film solar cells or infrared sensors [31]. The partial substitution of Se by S also makes it possible to optimize the position of the Fermi level and adapt the density of electronic states around the gap, thereby influencing the mobility of charge carriers [32].From a thermodynamic perspective, studies on similar materials such as $AgGaS_2$ show anisotropic behavior in terms of thermal expansion and thermal conductivity; for example, $AgGaS_2$ exhibits negative thermal expansion along the c-axis, with expansion coefficients varying depending on the crystallographic axes [33].Furthermore, investigations using modeling of vibrational and thermodynamic phenomena (via the quasi-harmonic approximation) reveal that thermal conductivity can be reduced under external pressure, while quantities such as Helmholtz free energy, entropy, and heat capacity (Cv) change significantly with temperature and pressure in $AgGaS_2$ systems [34].

The theoretical principles of the calculation are presented in Based on this principle, $AgAl(S_{1-x}Se_x)_2$ quaternary alloys can be studied in detail and comprehensively in order to optimize their properties according to chemical composition. It is important to note that this system has not yet been studied. This research aims to analyze the structural, electronic, optical, thermal, and thermodynamic properties of $AgAl(S_{1-x}Se_x)_2$ quaternary alloys. The first part also addresses the concept of the FP-LAPW method and the fundamentals of density functional theory (DFT). The second part presents the results obtained, their analysis, a discussion, and a comparison with various theoretical and experimental studies found in academic publications. Finally, the main conclusions are summarized in an overall summary.

## 2.COMPUTATIONAL DETAILS

We perform our calculations using the linearized augmented plane wave method and the local orbital technique (FP-LAPW+lo) [35]. This process provides a self-consistent solution to the Kohn-Sham equations, falling within the framework of density functional theory (DFT) [36, 37]. These techniques are applied in the WIEN2k code [38-40]. The generalized gradient approximation (GGA) function of Wu and Cohen (WC) [41] was used to treat the exchange and correlation potential. This method is also used to determine structural characteristics, with the aim of broadening and contrasting the various results obtained [42]. It should be noted that the GGA method tends to overestimate the lattice parameter while underestimating the band gap energies. The recent design of the Tran-Blaha technique based on the modified Becke-Johnson potential (TB-mBJ) parameterized by Koller et al. [43] represents an optimal and useful approach for determining the electronic characteristics of materials. The unit cell is divided into two zones: the first comprises non-overlapping spheres centered on each atom with a radius of Rmt, while the second represents the interstitial zone.

The wave functions, electron densities, and potentials are formulated as the product of spherical harmonics multiplied by radial functions around the atomic sites, i.e., in muffin-tin spheres with a cutoff radius $L_{max}$ = 10. They are also represented by Fourier series in the interstitial zone with a cutoff radius $R_{mt}\times K_{max}$ = 6 (where RMT denotes the smallest radius of the MT sphere and $K_{max}$ represents the amplitude of the largest wave vector used to expand the eigen functions of the plane wave). The separation between the core and valence electronic states is determined by an energy cutoff set at -6 Ry. In addition, we chose to set the Fourier expansion parameter $G_{max}$, which corresponds to the maximum reciprocal vector of the lattice responsible for accurately describing the charge density, to a value of 14. The iteration process is repeated until the total energy reaches stability at $10^{-5}$ Ry. The standard Monkhorst and Pack (MP) special point approach [44] was analyzed to obtain accurate Brillouin zone (BZ) integrations. For each group of 16 atoms, the k-mesh for the zinc-blende phase consisted of 7×7×4 K special points (12 K special points located in the irreducible corner of the Brillouin zone). To ensure correct convergence of the results, the choice was made on the k-meshes and basis sets.

## 3.RESULTS AND DISCUSSIONS

### 3.1. Structural properties

The structural stability of the quaternary alloy $AgAl(S_{1-x}Se_x)_2$ was investigated by optimizing the equilibrium lattice parameters (*a* and *c*) and the bulk modulus (*B*) for Se concentrations ranging from $x = 0$ to 1. A periodically repeated 16-atom ordered supercell was employed, where one, two, and three sulfur atoms were replaced by selenium for $x = 0.25$, 0.50, and 0.75, respectively (Fig. 1). This approach, widely used in first-principles studies of semiconductor alloys, efficiently captures the main effects of S/Se substitution on the structural, electronic, optical, and thermodynamic properties. Although real alloys exhibit substitutional disorder, the present calculations represent ordered configurations and should therefore be regarded as describing the general compositional trends. More advanced approaches, such as Special Quasirandom Structures (SQS) or the Coherent Potential Approximation (CPA), could provide a more realistic description of chemical disorder and are left for future work.

The equilibrium structure of each composition was determined by total-energy minimization through optimization of the internal parameter (*u*) and the *c/a* ratio. Here, u is the anion internal displacement parameter, which describes the deviation of the anion from its ideal tetrahedral position in the chalcopyrite structure and characterizes the distortion of the cation–anion tetrahedra. Since u directly affects the bond lengths and electronic structure, its optimization is essential for obtaining reliable structural and electronic properties.

For the parent compounds $AgAlS_2$ and $AgAlSe_2$, the optimized value of *u* was found to be in good agreement with the available experimental data and was therefore adopted in the subsequent calculations.

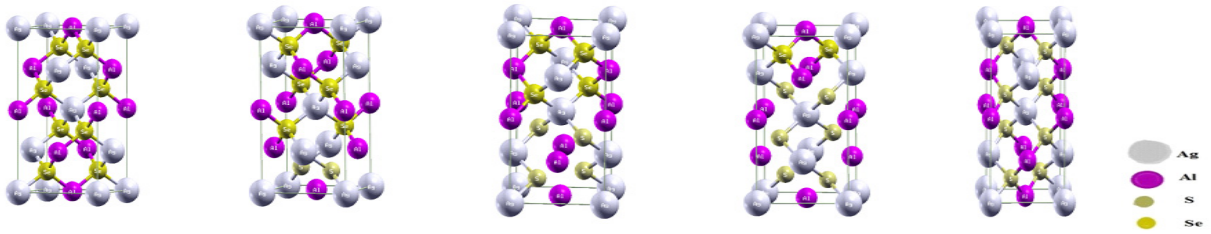


**Figure 1**. Cell structure of the five alloys $AgAl(S_{1-x}Se_x)_2$

The optimized structural parameters are summarized in Table 1. No theoretical or experimental data for the $AgAl(S_{1-x}Se_x)_2$ quaternary alloys are currently available in the literature, making the present results a valuable reference for future investigations. For the compounds $AgAlS_2$ and $AgAlSe_2$, the calculated lattice constants (a and c) and the corresponding c/a ratios are in excellent agreement with the available experimental data, with deviations of only 0.17% and 1.02% for $AgAlS_2$, and 1.56% and 0.50% (or 1.80% and 0.56%, depending on the experimental reference) for $AgAlSe_2$. These small discrepancies confirm the high accuracy of the present computational approach and validate the reliability of the predicted structural properties.

**Table 1.** The equilibrium constants, calculated as a, c, and the compressibility modulus B for $AgAl(S_{1-x}Se_x)_2$, are compared with existing experimental and theoretical data.

| Compounds | Methods | *a*(Å) | *c*(Å) | *u* | *B*(GPa) | $E_{tot}$(eV) |
|---|---|---|---|---|---|---|
| $AgAlS_2$ | Present work | 5.60 | 10.49 | 0.29 | 79.22 | -50857.60 |
| | Experiment | 5.72 [a]<br>5.69 [b]<br>5.13 [e] | 10.13 [a]<br>10.26 [b]<br>10.30 [e] | 0.29 [a]<br>0.30 [b]<br>0.30 [e] | 78, 70 [c] | |
| | Other work | 5.48 [f] | 10.90 [f] | 0.256 [f] | - | - |
| $AgAlS_{0.25}Se_{0.75}$ | Present work | 5.65 | 10.72 | 0.29 | 73.69 | -58980.91 |
| | Experiment | - | - | - | - | - |
| | Other work | - | - | - | - | - |
| $AgAlS_{0.5}Se_{0.5}$ | Present work | 5.83 | 10.45 | 0.29 | 70.59 | -67104.03 |
| | Experiment | - | - | - | - | - |
| | Other work | - | - | - | - | - |
| $AgAlS_{0.75}Se_{0.25}$ | Present work | 5.81 | 10.96 | 0.29 | 67.46 | -67104.03 |
| | Experiment | - | - | - | - | - |
| | Other work | - | - | - | - | - |
| $AgAlSe_2$ | Present work | 5.89 | 11.07 | 0.28 | 64.45 | -83350.31 |
| | Experiment | 5.95 [a]<br>5.95 [b]<br>5.96 [d] | 10.75 [a]<br>10.75 [b]<br>10.75 [d] | 0.27 [a]<br>0.27 [b] | 78, 70 [c] | |
| | Other work | 5.78 [f] | 11.52 [f] | 0.263 [f] | - | - |

Ref: [a][24], [b][45], [c][46], [d][29], [e][47], [f][28].

Figure 2 presents the variation of the crystal volume as a function of the Se concentration x for the quaternary alloy $AgAl(S_{1-x}Se_x)_2$. For comparison, the volume predicted by Vegard's law [48] is also included in figure. It can be

seen that the crystal volume deviates positively or negatively from linearity. For an $AgAl(S_{1-x}Se_x)_2$ alloy compound, the volume of the crystal lattice is formulated as follows:

$$V_{ABC_{1-x}D_x} = x.V_{ABC} + (1-x)\cdot V_{ABD}. \quad (1)$$

Where $V_{ABC}$ and $V_{ABD}$ denote the equilibrium crystal volumes of the ternary compounds ABC and ABD, respectively. For the $AgAl(S_{1-x}Se_x)_2$ alloys, the fitted bowing parameter is found to be only 0.01 (a.u.)$^3$, indicating a negligible deviation from the linear behavior predicted Vegard's law. We observe that the alloys analyzed comply with Vegard's law. This phenomenon can be explained by the slight modification of the lattice parameters of the parent ternary compounds constituting the alloy.

In the same figure the variation in compressibility coefficient in relation to concentration for $AgAl(S_{1-x}Se_x)_2$ systems. A comparison is made between the graphs obtained and those derived from the linear concentration dependence (LCD) law. A small divergence is noted in the change in the compressibility modulus in relation to concentration compared to the LCD, with a curvature index of 5.72 GPa. This small difference is mainly attributed to the slight disparity between the compressibility modulus values of the ternary compounds. It is observed that the compressibility modulus decreases as the atomic number of the substitution chalcogenide increases.

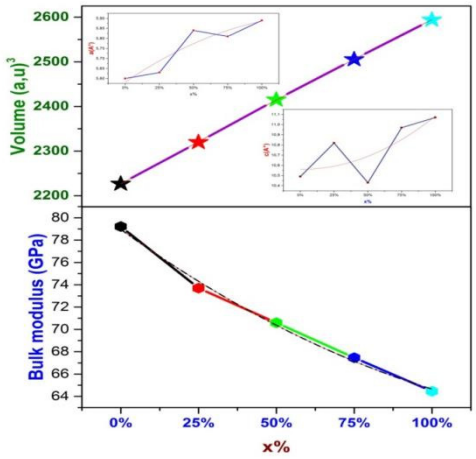


**Figure 2**. Variation in volume and compressibility modulus in relation to concentration, and comparison with Vegard's law for ideal ternary compounds. $AgAlS_2$ and $AgAlSe_2$

### 3.2. Electronic properties

The band gap is often considered a crucial criterion in the selection of a semiconductor element for optoelectronic applications, given its direct link to the wavelength at which the device operates. In this context, the dependence of the fundamental band gap on the alloy composition is of paramount importance. Thus, the electronic characteristics of $AgAl(S_{1-x}Se_x)_2$ quaternary alloys are examined, taking into account the lattice parameters that have been previously optimized.

The band structure was established along the high symmetry directions in the Brillouin zone. To refine the accuracy of the band gap values, in addition to the WC-GGA approximation, the mBJ approximation was also used. This method is known to provide band gap values that rival those measured experimentally. For the alloys analyzed, the valence band peak and the conduction band trough are located at the Γ point (see Figure 3). allows them to be classified as direct bandgap semiconductors. Table 2 presents the results for these alloys at concentrations of x = 0, 0.25, 0.50, 0.75, and 1. It also includes experimental and theoretical data for ternary compounds.

**Table 2.** The calculated band gaps of $AgAl(S_{1-x}Se_x)_2$

| Compounds | Present work | | Experimental | Other work |
|---|---|---|---|---|
| | WC-GGA | mBJ | | |
| $AgAlS_2$ | 1.787 | 3.202 | 3.13[a], 3.186[b] | 1.87[c], 2.69[c], 1.98[d] |
| $AgAlSe_{0.75}S_{0.25}$ | 1.616 | 2.935 | - | - |
| $AgAlSe_{0.50}S_{0.50}$ | 1.424 | 2.766 | - | - |
| $AgAlSe_{0.25}S_{0.75}$ | 1.214 | 2.589 | - | - |
| $AgAlSe_2$ | 1.038 | 2.412 | 2.55[a] | 0.98[c] 1.8[c], 1.59[e] |

Ref: [a][49], [b][50], [c][51], [d][45] , [e][46]

This study only compares its results with existing experimental and theoretical data for ternary alloys, due to the lack of experimental information for the quaternary system. It should be noted that the band gap energy values determined using the WC-GGA method are lower than the expected experimental results. It is well known that DFT is a ground state-based technique and is not capable of reproducing excited states. However, the use of the mBJ approximation prevents us from accurately determining the band gap value. Figure 4 illustrates how the band gap of $AgAl(S_{1-x}Se_x)_2$ quaternary alloys varies as a function of concentration x.

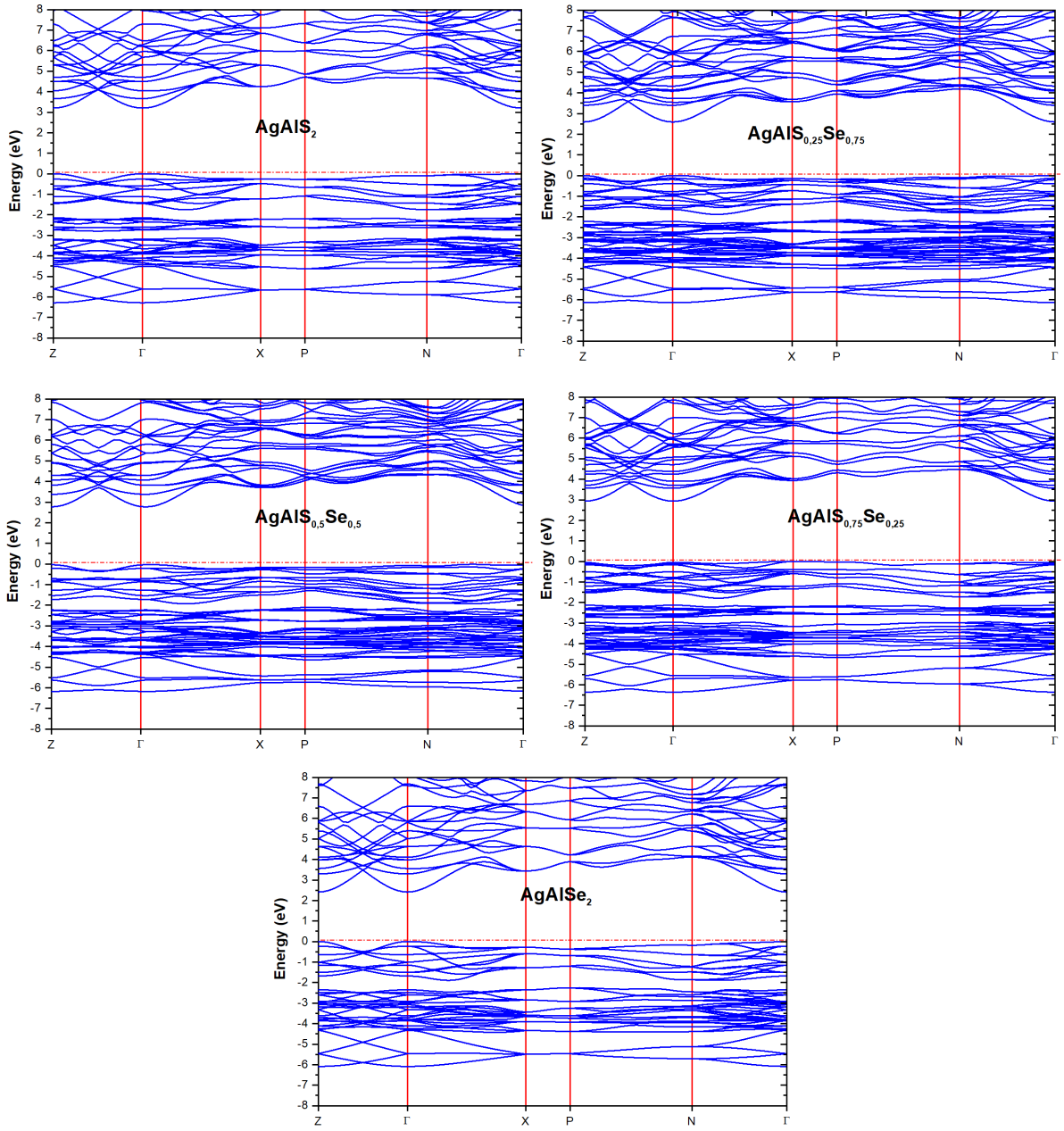


**Figure 3**. Band Structure of $AgAl(S_xSe_{1-x})_2$ alloys

The mBJ results indicate that the band gap energy decreases as a function of Se concentration, following a nonlinear trend. The curves represent a quadratic fit. It has been proven that the curvature parameter is mainly attributed to the difference between the lattice parameters and the ionic elements of the original ternary compounds [52, 53]. For a better understanding and explanation of the physical origins of the curvature parameter, the method developed by Bernard and Zunger [54] was adopted. This approach comprises three distinct elements that form the disorder parameter b: volume deformation ($b_{VD}$), charge transfer ($b_{CE}$), and structural relaxation ($b_{SR}$).

The calculations were restricted to a concentration of x = 0.5 due to the weak dependence of the curvature parameter on chemical composition. The first task is to determine the influence of volume deformation ($V_D$) on the disorder parameter. The comparative response of the band structures of the ternary compounds ABC and ABD to hydrostatic pressure is illustrated by their corresponding $b_{VD}$ contribution. In this context, this response stems from the

adjustment of their specific structural configurations relative to those of the alloy V = V (x) (Vegard's law). The second contribution concerns charge transfer (CE), where the contribution $b_{CE}$ summarizes the impact of charge transfer attributed to the behavior of atomic bonds on the value of the structural parameter a.The final step involves evaluating the variation caused by structural relaxation ($S_R$), from the unrelaxed alloy to the relaxed alloy by $b_{SR}$. Consequently, the total disorder parameter is obtained by combining these three elements.

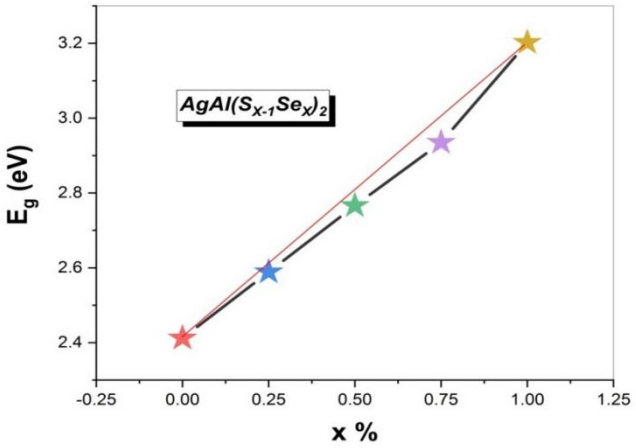


**Figure 4**. Variation of gap energy with concentration and comparison with Vegard's law

### 3.3. Optical properties

The complex dielectric function entirely determines the optical properties of materials, which are theoutcome of their interactions with electromagnetic waves and given by the following formula [55]

$$\varepsilon(\omega) = \varepsilon_1(\omega) + i\varepsilon_2(\omega). \tag{2}$$

Where $\varepsilon_1(\omega)$ and $\varepsilon_2(\omega)$ by using the Kramers–Kronig denote the real and imaginary parts of the dielectric function, respectively [55,56]

$$\varepsilon_1(\omega) = 1 + \frac{2}{\pi} P \int_0^{\infty} \frac{\omega' \varepsilon_2(\omega')}{\omega'^2 - \omega^2} d\omega'. \tag{3}$$

The following relations were used to calculate other optical quantities from $\varepsilon_1(\omega)$ and $\varepsilon_2(\omega)$, including the absorption coefficient $\alpha(\omega)$, the optical conductivity $\sigma(\omega)$, the refractive index $n(\omega)$, the extinction coefficient $K(\omega)$, the reflection coefficient R ($\omega$), and the absorption coefficient $\alpha(\omega)$ were calculated from $\varepsilon_1(\omega)$ and $\varepsilon_2(\omega)$ and are given by the following relations [57]:

$$n(\omega) = \frac{1}{\sqrt{2}}[(\varepsilon_1{}^2(\omega) + \varepsilon_2{}^2(\omega))^{\frac{1}{2}} + \varepsilon_1(\omega)]^{1/2}, \tag{4}$$

$$K(\omega) = \frac{1}{\sqrt{2}}[(\varepsilon_1{}^2(\omega) + \varepsilon_2{}^2(\omega))^{\frac{1}{2}} - \varepsilon_1(\omega)]^{1/2}, \tag{5}$$

$$\text{Re}\,\sigma(\omega) = \frac{\omega}{4\pi}\text{Im}\,\varepsilon(\omega), \tag{6}$$

$$\alpha(\omega)\frac{4\pi}{\lambda}\text{k}(\omega), \tag{7}$$

$$\text{R}(\omega) = \frac{(\text{n}-1)^2+\text{K}^2}{(\text{n}+1)^2+\text{K}^2}. \tag{8}$$

The physical properties of $AgAl(S_{1-x}Se_x)_2$ alloys with a tetragonal crystal structure and space group $D_{2d}^{12}$-$I\bar{4}2d$ require two shaded tensor components in the subfigures $\varepsilon^{xx}(\omega)$ and $\varepsilon^{zz}(\omega)$ to perform the calculations [57].

Figures 5.a and 5.b illustrate the evolution of real and imaginary parts of the dielectric function as a function of photon energy in both crystal directions for each alloy. The static dielectric constant $\varepsilon_1(0)$ increases, independently of the alloy composition, in the order of magnitude between 4.31 and 4.85 for $\varepsilon_{xx}(0)$ and between 4.46 and 5.01 for $\varepsilon_{zz}(0)$ (see Table 3). Consequently, the anisotropy of $AgAlSe_2$is the most significant.

The $\varepsilon_1(0)$ component is different from the other constituent $\varepsilon_{1xx}(0)$ for the same compound, which indicates that the optical anisotropy in the zz direction is the most significant. The zero crossing of $\varepsilon_1(\omega)$= 0 corresponds to the maximum of the imaginary part $\varepsilon_2(\omega)$. This is to be expected, since when dispersion is minimal, the absorption is maximal.

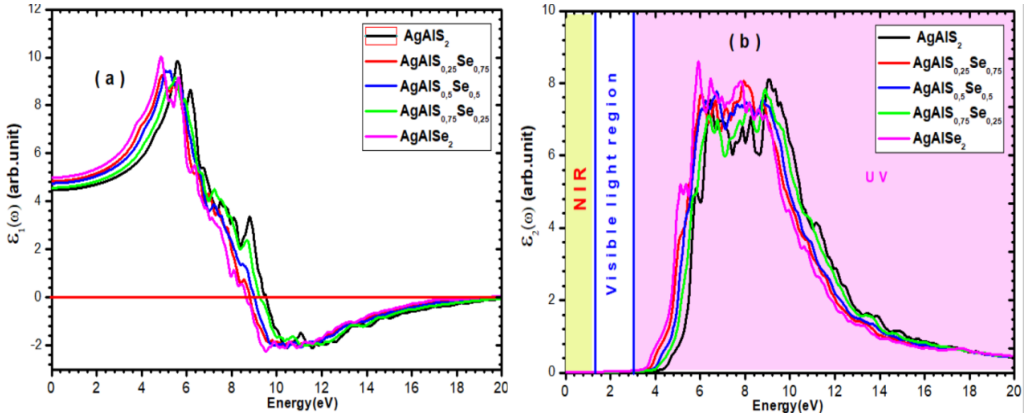


**Figure 5**. Real part(a) and imaginary part (b) of the dielectric function for $AgAl(S_xSe_{1-x})_2$ alloys

**Table 3.** Dielectric constant and refractive index (n) for $AgAl(S_{1-x}Se_x)_2$

| | $\varepsilon_1^{//}(0)$ | $\varepsilon_1^{\perp}(0)$ | $\varepsilon_{moy}$ | $n_1^{//}(0)$ | $n_1^{\perp}(0)$ | $\Delta n$ |
|---|---|---|---|---|---|---|
| $AgAlS_2$ | 4.31 | 4.46 | 4.385 | 2.11 | 2.07 | 0.04 |
| $AgAlSe_{0.75}S_{0.25}$ | 4.57 | 4.49 | 4.53 | 2.12 | 2.13 | 0.01 |
| $AgAlSe_{0.50}S_{0.50}$ | 4.77 | 4.51 | 4.64 | 2.12 | 2.17 | 0.05 |
| $AgAlSe_{0.25}S_{0.75}$ | 4.72 | 4.83 | 4.775 | 2.17 | 2.20 | 0.03 |
| $AgAlSe_2$ | 4.85 | 5.02 | 4.935 | 2.19 | 2.23 | 0.06 |

Table 3 presents the static dielectric constants $\varepsilon_1(0)$, the average dielectric constant $\varepsilon_{moy}$, the static refractive indices n(0), and the birefringence $\Delta n$ of $AgAl(S_{1-x}Se_x)_2$ alloys. The obtained results reveal a systematic evolution of the optical response with increasing Se concentration, reflecting the modification of the electronic polarization induced by the substitution of S with Se.

The static dielectric constant exhibits a gradual increase with increasing Se content in both crystallographic directions. Specifically, $\varepsilon_1//(0)$ increases from 4.31 for $AgAlS_2$ to 4.85 for $AgAlSe_2$, while $\varepsilon_1\perp(0)$ increases from 4.46 to 5.02. Consequently, the average dielectric constant rises continuously from 4.385 to 4.935, corresponding to an enhancement of approximately 12.5%. This behavior is mainly attributed to the higher electronic polarizability of Se atoms compared with S atoms, as well as to the progressive reduction of the electronic band gap. According to the Penn model, the static dielectric constant is inversely proportional to the square of the band gap; therefore, the decrease in $E_g$ naturally leads to stronger dielectric screening and higher dielectric constants.

The static dielectric constant was estimated using the Penn model, which relates the dielectric response to the band gap and the plasma frequency [58]:

$$\varepsilon(0) = 1 + \left(\frac{\hbar\omega_p}{E_g}\right)^2. \quad (9)$$

Where $\hbar$ is the reduced Planck constant, $E_g$ is the fundamental band gap, and $\omega_p$ is the plasma frequency, which characterizes the collective oscillation of the valence electrons in the material. The values of $\varepsilon_1(0)$ and $\varepsilon_{1zz}(0)$ are listed in Table 3.

Figure 6.a illustrates the absorption $\alpha(\omega)$ of $AgAl(S_{1-x}Se_x)_2$alloys. It is clear that the spectra of $AgAlSe_2$ have the highest intensity and the shortest width at half height $\Delta\omega$. The optical conductivity curves show the same results (Fig. 6.b), with the conductivity threshold beings lightly lower than the band gap value. These results can be explained by the fact that optical conductivity is due to inter band transitions on the one hand and intra band transitions on the other.

The variation of the refractive index $n(\omega)$ is illustrated in Figure 6c. It can be seen a variation of $n(\omega)$ between the three compounds follows the same trend as the spectrum of $\varepsilon_1(\omega)$. This is evident from the static refractive index n(0) values of 2.05, 2.12, and 2.23 for $AgAl(S_{1-x}Se_x)_2$, respectively. This value is located in the static limit and follows the relationship:

$$n(\omega) = \sqrt{\varepsilon(0)}. \quad (10)$$

The reflectivity spectra (Fig. 6.e) demonstrate a low reflected intensity in the strong absorption interval, and its decrease coincides with the minimum of the real part $\varepsilon_1(\omega)$. The spectra of the energy-loss function, shown in Figure 6.f, reflect the energy-loss of fast electrons as they pass through the material and the plasma resonance frequency $\omega_p$ [59] is also observed in the reflectivity spectrum.

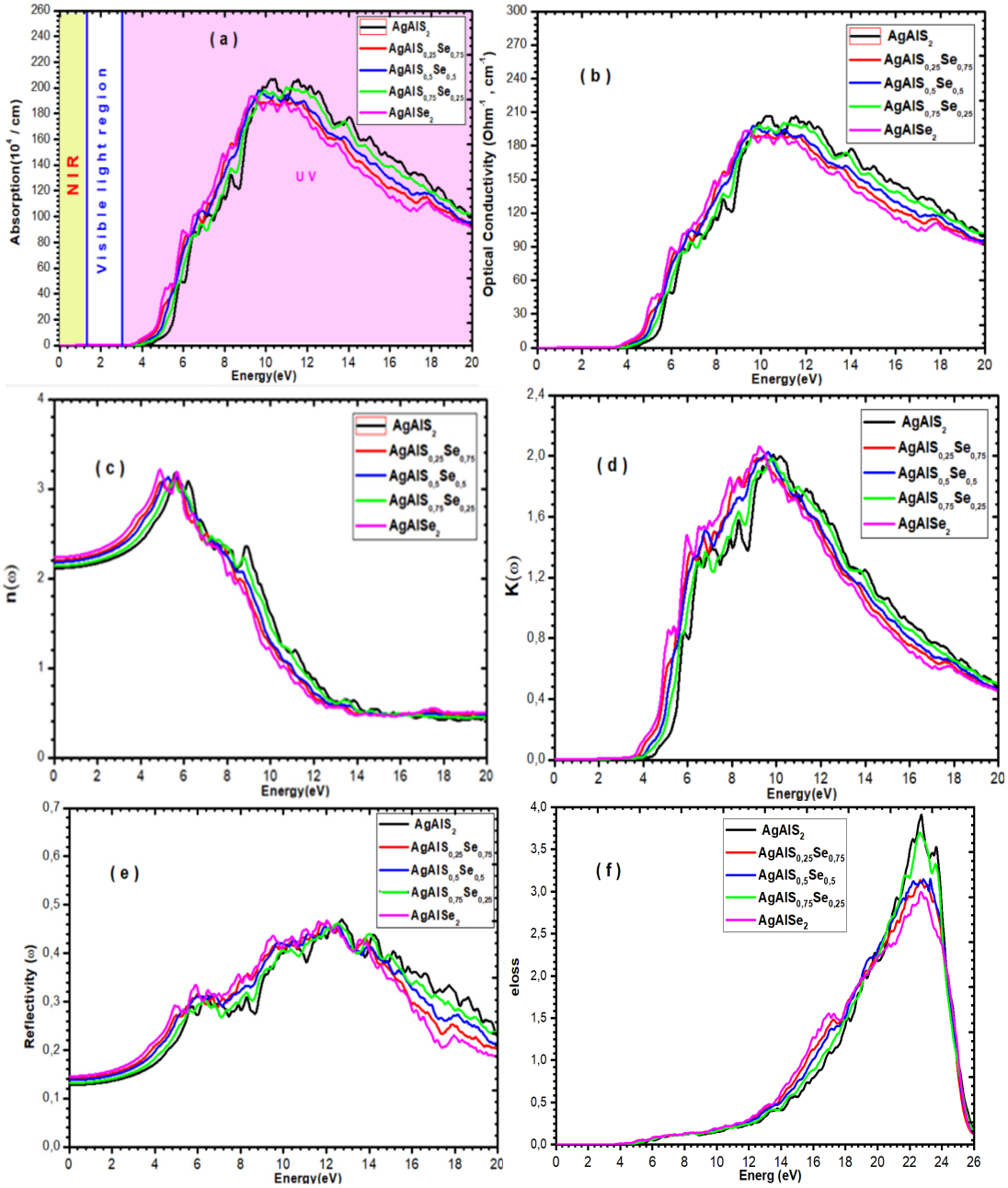


**Figure 6**. Calculated optical properties of $AgAl(S_xSe_{1-x})_2$ alloys:
(a) absorption coefficient (α), (b) optical conductivity (σ), (c) refractive index (n), (d) extinction coefficient (k), (e) reflectivity (R), and (f) energy-loss function (L), as functions of photon energy.

### 3.4. Thermodynamic properties

The thermodynamic properties of $AgAl(S_{1-x}Se_x)_2$ alloys were studied using the Debye quasi-harmonic model (QHDM) based on the FP-LAPW method. While density functional theory (DFT) provides an accurate description of the ground-state properties at 0 K, the quasi-harmonic Debye approximations can be used to extend these calculations at finite temperatures and pressures by incorporating the vibrational contribution to the free energy.

The properties at specific temperatures and pressures are obtained from the Gibbs energy of non-equilibrium systems as follows: [60]

$$G(V, P, T) = E(V) + PV + A_{vib}(V, T). \tag{11}$$

Where E(V) is the total energy, P is the external pressure, V is the crystal volume, and $A_{vib}$ is the Helmholtz vibrational free energy calculated using the Debye approximation.

For each temperature and pressure, the equilibrium volume was obtained by minimizing the Gibbs free energy according to the condition: [61]

$$\left(\frac{\partial G}{\partial V}\right)_{P,T} = 0. \tag{12}$$

The variation in crystal volume as a function of temperature at different pressures for quaternary $AgAl(S_{1-x}Se_x)_2$ alloys is illustrated in Figure 7. It is clear that as the temperature increases, the volume also increases, but the rate of this increase is moderate as the pressure increases. However, for a given temperature, the volume decreases as the pressure increases. Furthermore, it is noted that the volume is almost constant in the temperature range 0-800 K with a setting in the range 0-20 GPa. The expansion of volume V ($bohr^3$) is almost negligible above this temperature.

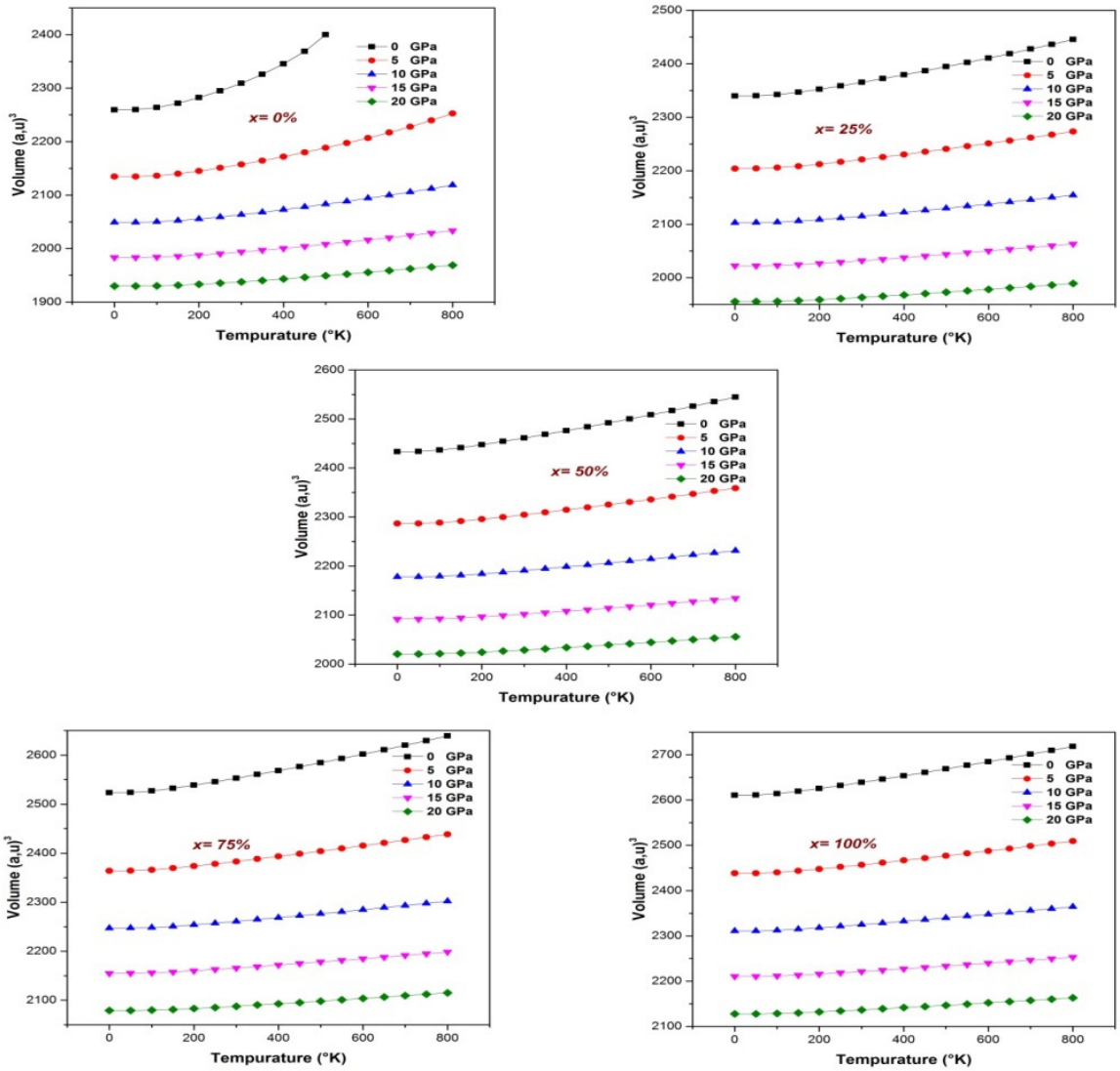


**Figure 7**. Volume as a function of temperature at various pressures

The same trend can be observed in the evolution of the compressibility modulus B of $AgAl(S_{1-x}Se_x)_2$alloys as a function of temperature and pressure variations; see Figure 8. It can be seen that at a given temperature, the compressibility modulus increases with pressure, but it decreases at a given pressure. However, the rate of increase in the compressibility modulus as a function of temperature is greater at low pressure, because at these pressures, the compressibility modulus is higher.

The Debye temperature $\theta_D$ is a crucial fundamental parameter in solids that is connected to physical characteristics, including specifiche at and melting temperature [62]:

$$\theta_D = \frac{\hbar}{k_B}\left(\frac{6\pi^2 n}{V}\right)^{1/3} f(\sigma)\sqrt{\frac{B_S}{M}}. \tag{13}$$

Where n is the number of atoms per formula unit, V is the molecular volume, $B_S$ is the adiabatic bulk modulus, M is the molecular mass per formula unit, f(σ) is a function of Poisson's ratio σ, $\hbar$ is the reduced Planck constant, and $k_B$ is the Boltzmann constant.

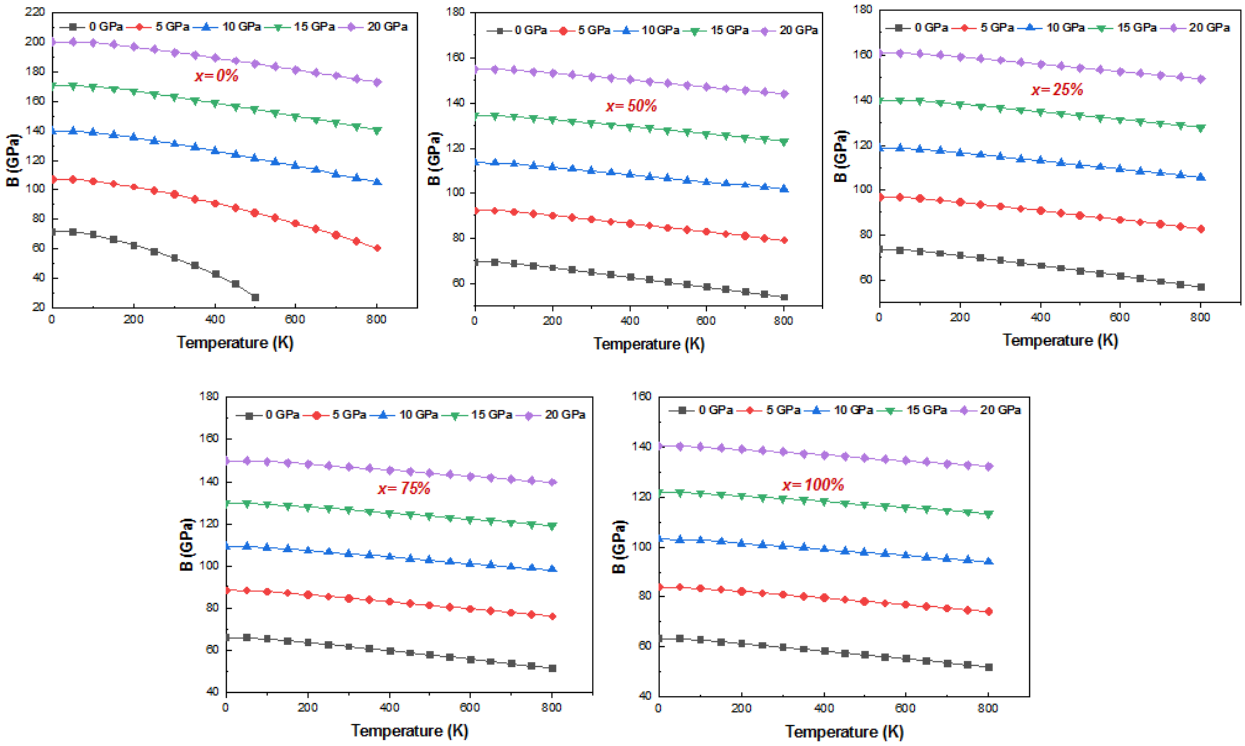


**Figure 8**. Bulk modulus as a function of temperature at various pressures.

$B_S$ is the static adiabatic bulk modulus determined by the relation [63] and M is the molecular mass per unit cell:

$$B_S \cong B(V) = V\frac{d^2E(V)}{dV^2} \tag{14}$$

and $f(\sigma)$ is a function of the Poisson ratio $\sigma$ expressed as [64]:

$$|f(\sigma)|^3 = 3\left[2\left(\frac{2}{3}\frac{1+\sigma}{1-2\sigma}\right) + \left(\frac{1}{3}\frac{1+\sigma}{1-\sigma}\right)\right]^{-1} \tag{15}$$

where $\sigma$ is taken as 0.25 [65].

In the present work, a constant Poisson's ratio (σ = 0.25) was adopted for all alloy compositions within the quasi-harmonic Debye model. This approximation is commonly used in first-principles thermodynamic studies when the complete set of elastic constants is unavailable and provides a reasonable description of the average elastic behavior of semiconductor alloys. Although the Debye temperature depends on Poisson's ratio, moderate variations in σ have only a minor influence on the calculated thermodynamic properties compared with the effects of the equilibrium volume and bulk modulus [66]. Therefore, the use of a constant value of σ = 0.25 is expected to preserve the overall compositional trends and the main conclusions of this work.

The variation of the Debye temperature $\theta_D$ as a function of temperature at different pressures for the materials studied is illustrated in Figure 9. When the pressure is constant, the Debye temperature decreases almost linearly with increasing temperature, and at a given temperature, the Debye temperature increases with the applied pressure. This behavior has been observed in the evolution of the compressibility modulus when temperature and pressure vary. This is explained by the fact that a hard material has a high Debye temperature. Research on the heat capacity of crystals is well known in the field of condensed matter physics [67].

The heat capacity of a substance provides important information about its vibrational characteristics and is required in many applications. Figure 10 graphically illustrates how the heat capacityat constant volume $C_V$ varies with temperature at different pressures for the $AgAl(S_{1-x}Se_x)_2$ alloys studied. Following the example of the Debye temperature parameter, there are two steps observed:

At high temperatures, the value of $C_V$ tends towards the limit of Dulong-Petit, which all solids exhibit when heated at high temperatures. From Fig. 10, when the temperature increases, the value of $C_V$ increases drastically at low temperatures, then the increase becomes slow at high temperatures until reaching the limit of Dulong-Petit as expected by theory. The $C_V$ values obtainedat T = 300 K and P = 0 GPa are 371.56, 369.39, 373.72, 376.91, and 379.07 J/mol.K for $AgAlS_2$, $AgAlS_{0.25}Se_{0.75}$, $AgAlS_{0.5}Se_{0.5}$, $AgAlS_{0.75}Se_{0.25}$, and $AgAlSe_2$, respectively.

For the variation of the heat capacity at constant pressure $C_p$ as a function of temperature at different pressures for the $AgAl(S_{1-x}Se_x)_2$systems, as shown in Fig. 11, it can be seen that at low temperature, $C_p$ behaves similarly to $C_V$, i.e.,

an evolution in $T^3$. But at high temperatures, $C_p$ behaves differently than $C_V$; rather than trending toward a constant value, it keeps rising. At 300K and atzero pressure, the obtained values for $C_p$ are 427.63, 466.32, 489.81, 513.58, and 532.54 J/mol.K for $AgAlS_2$, $AgAlS_{0.25}Se_{0.75}$, $AgAlS_{0.5}Se_{0.5}$, $AgAlS_{0.75}Se_{0.25}$, and $AgAlSe_2$, respectively. It is noted that pressure does not have a significant effect on heat capacity. Where the heat capacity $C_v$ and the Grüneisen parameter $\gamma$ are calculated with the following relations [60]:

$$C_V = 3nk_B\left[4D\left(\frac{\theta_D}{T}\right) - \frac{3\theta_D/T}{e^{\theta_D/T}-1}\right], \tag{16}$$

$$\gamma = \frac{-dln\theta_D(V)}{dlnV}. \tag{17}$$

In the above expressions, D(x) denotes the Debye function, defined as:

$$D(x) = \frac{3}{x^3}\int_0^x \frac{t^3}{e^t-1}\,dt, \tag{18}$$

where $= \frac{\theta_D}{T}$, $\theta_D$ is the Debye temperature, and T is the absolute temperature. The Debye function accounts for the contribution of lattice vibrations to the thermodynamic properties within the quasi-harmonic Debye approximation.

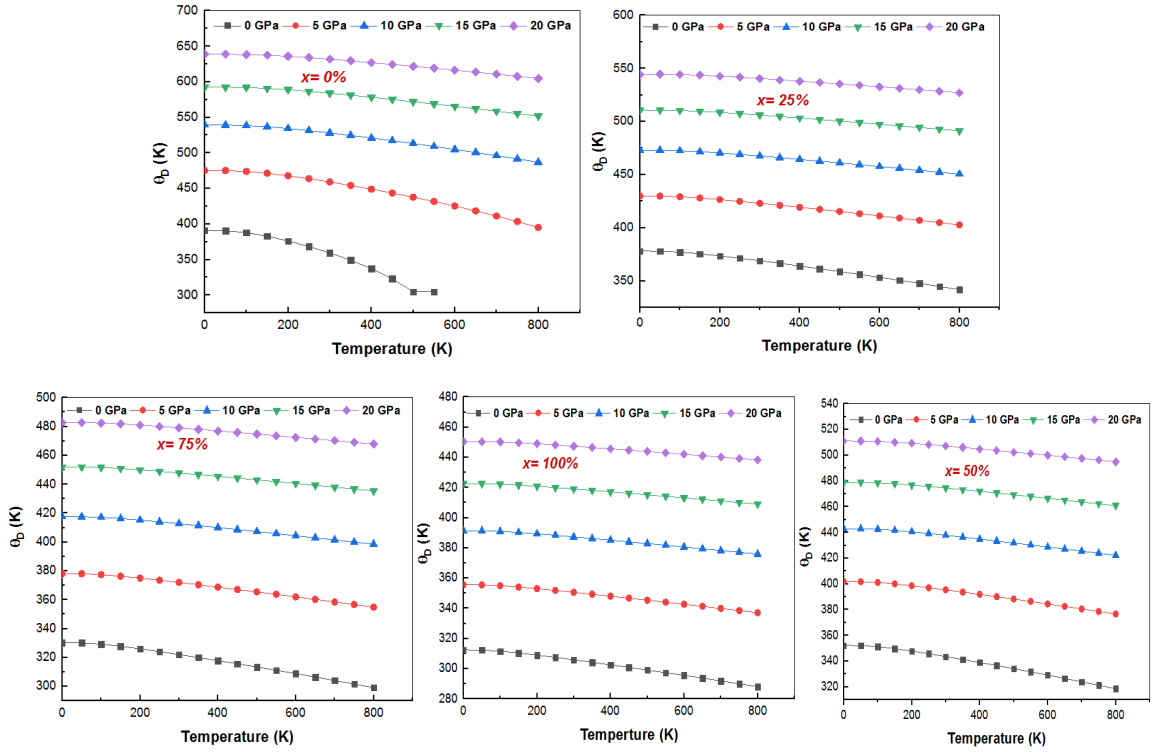


**Figure 9**. Debye temperature as a function of temperature at various pressures

The thermal expansion coefficient α indicates the dependence of volume on temperature at constant pressure:

$$\alpha = \frac{\gamma C_V}{B_T V}. \tag{19}$$

The variation of the thermal expansion coefficient, α as a function of temperature at different pressures for the investigated $AgAl(S_{1-x}Se_x)_2$ alloys is represented in Fig. 12. It is noted that, at a given pressure, the coefficient of thermal expansion α increases sharply for low temperatures (up to 800 K) irrespective of the alloy composition. When the temperature is greater than 800 K, the coefficient of thermal expansion α exhibits an approximately linear dependence trend and the increase rate becomes moderate, indicating that the temperature dependence of α is negligible for high temperatures. At high temperature and pressure, the coefficient of thermal expansion tends to converge towards a constant value.

The entropy S describes the distribution of matter and energy. Entropy is a metric used to quantify the disorder of a system. It has the following relation [19, 67]:

$$S = nk_B\left[4D\left(\frac{\theta_D}{T}\right) - 3ln\left(1-e^{-\theta_D/T}\right)\right]. \tag{20}$$

The variation of the entropy $S$ with respect to temperature and pressure is presented in Fig. 13. The entropy increases sharply with increasing temperature but decreases with increasing pressure. The calculated values of entropy at $T$ = 800 K and $P$ = 0 GPa are 813.80, 869.26, 897.84, 923.88, and 936.89 J/mol.K for $AgAlS_2$, $AgAlS_{0.25}Se_{0.75}$, $AgAlS_{0.5}Se_{0.5}$, $AgAlS_{0.75}Se_{0.25}$, and $AgAlSe_2$, respectively.

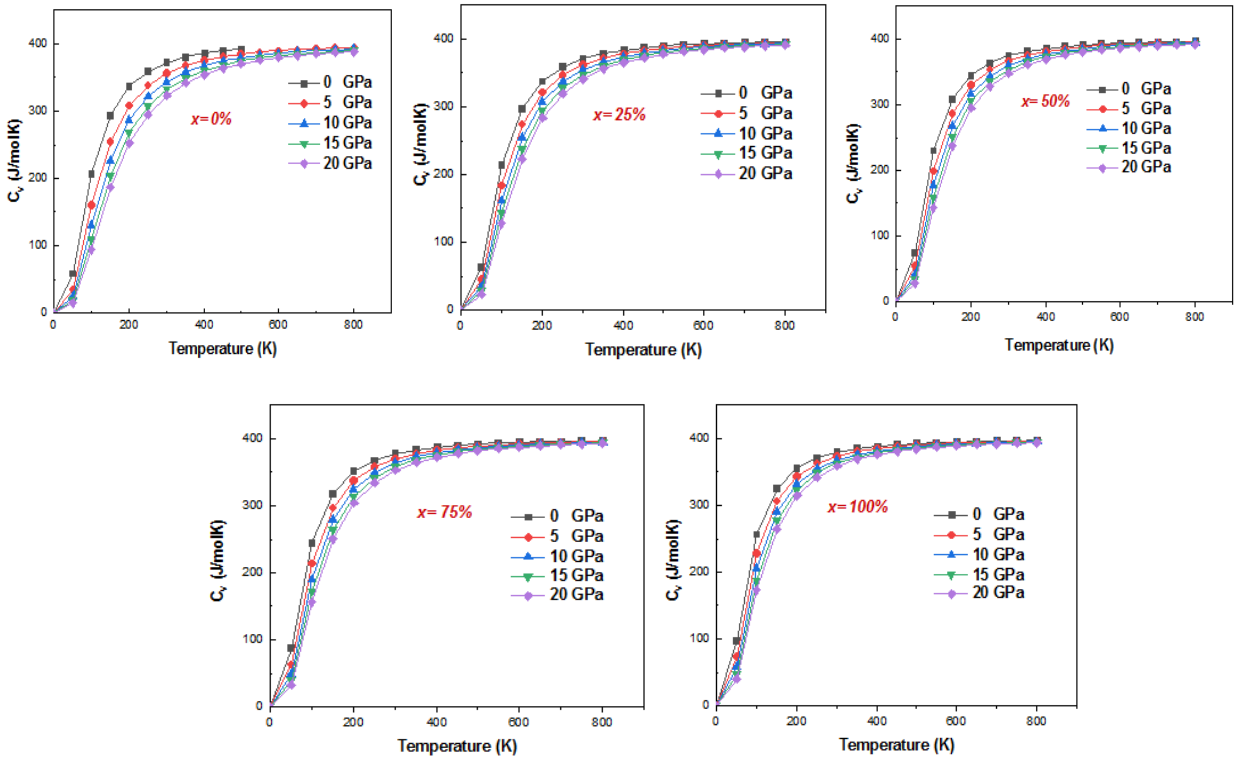


**Figure 10**. Heat capacity $C_V$ as a function of temperature at various pressures

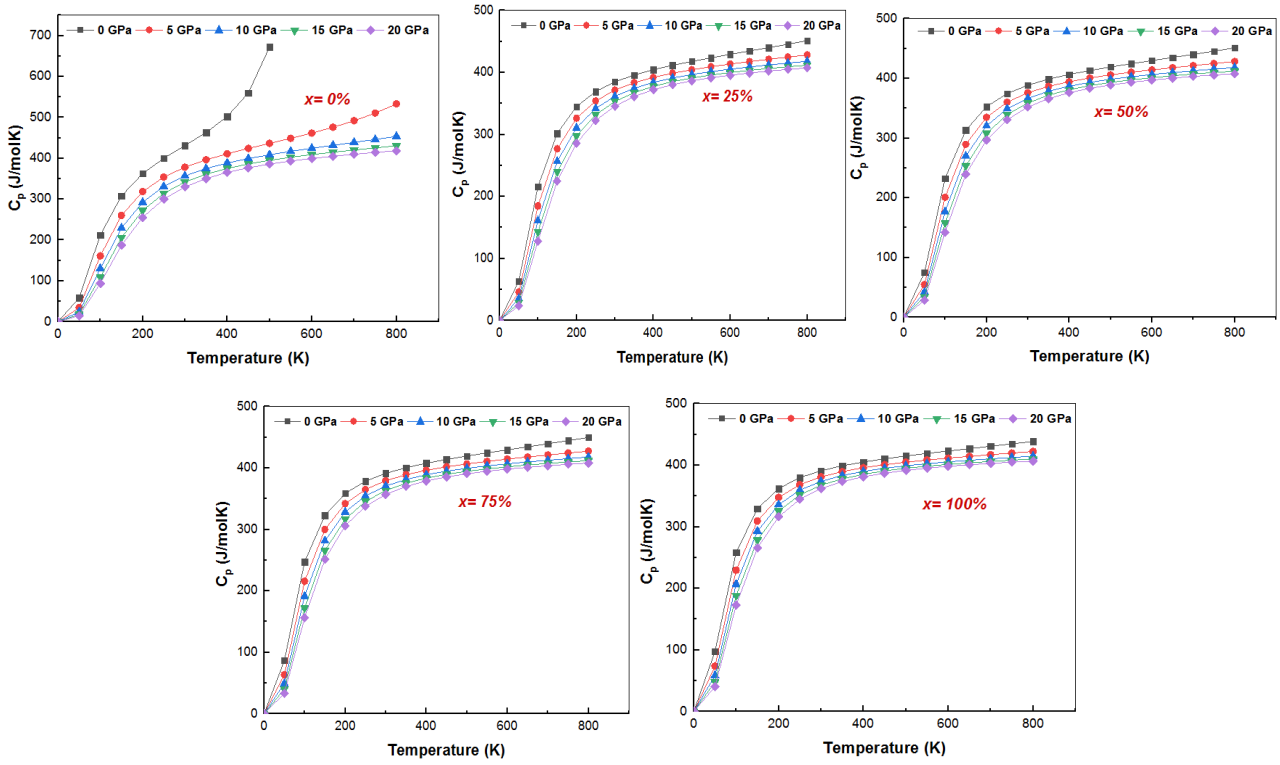


**Figure 11**. Heat capacity $C_P$ as a function of temperature at various pressures.

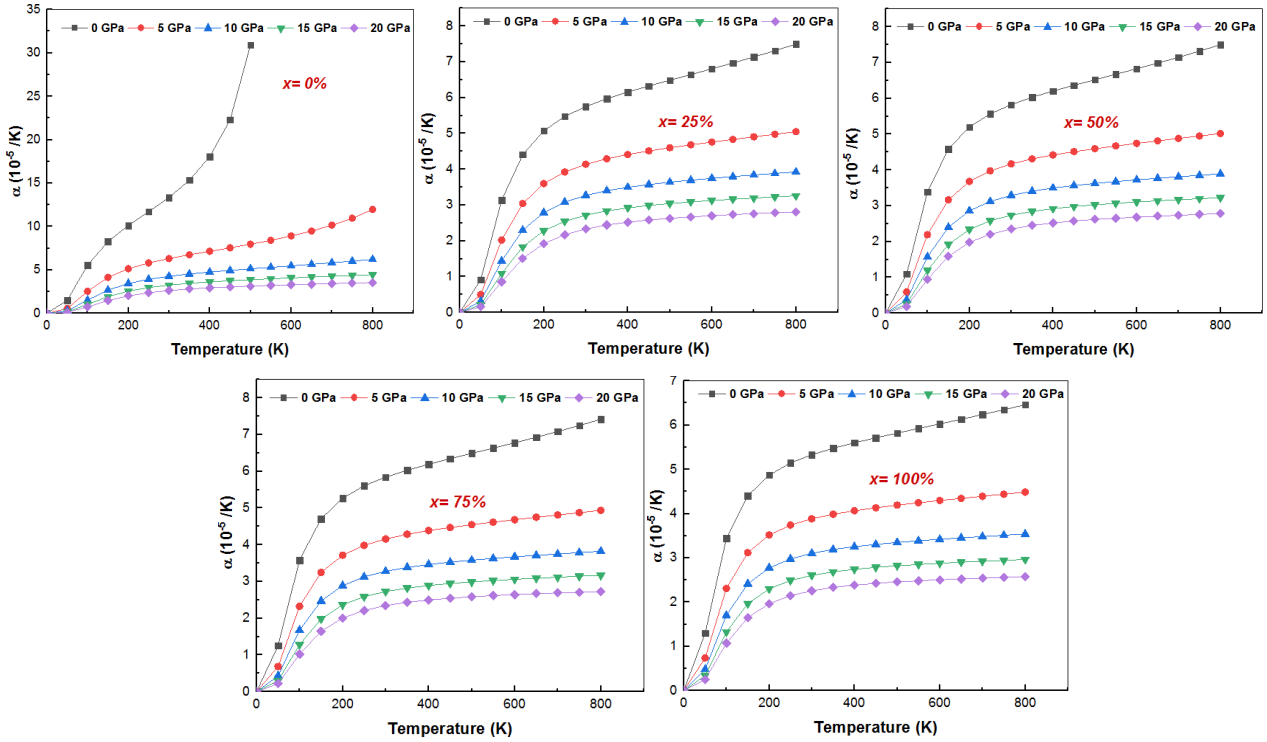


**Figure 12**. Thermal expansion coefficient as a function of temperature at various pressures

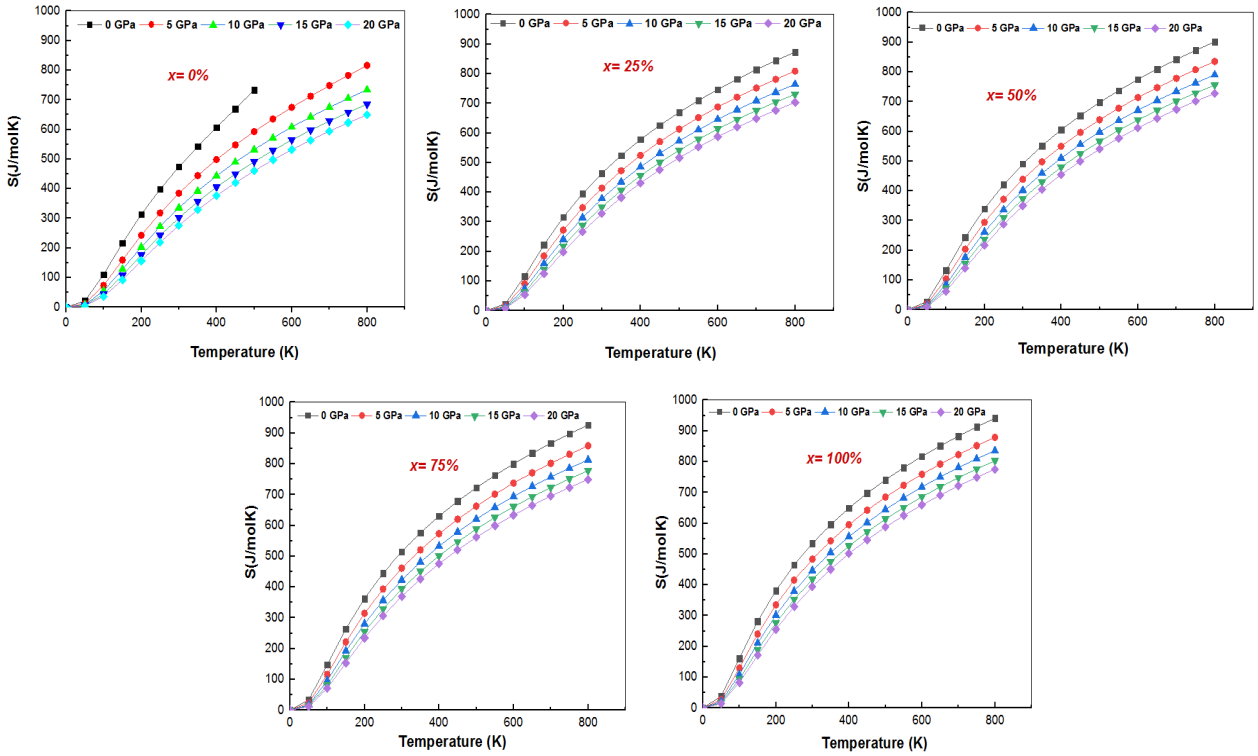


**Figure 13**. Entropy S as a function of temperature at various pressures

## 4. CONCLUSIONS

In conclusion, the structural, electronic, optical, and thermodynamic properties of $AgAl(S_{1-x}Se_x)_2$ quaternary alloys were systematically investigated using the all-electron FP-LAPW method within the framework of density functional theory. The calculated structural parameters are in good agreement with available theoretical and experimental data, confirming the reliability of the computational approach. The lattice parameters exhibit a nearly linear dependence on Se concentration, in accordance with Vegard's law, whereas the bulk modulus shows a noticeable deviation from linear

concentration dependence. Electronic structure calculations based on the modified Becke–Johnson (mBJ) potential reveal that both the parent compounds and the quaternary alloys are direct-band-gap semiconductors with the valence-band maximum and conduction-band minimum located at the Γ point. The nonlinear evolution of the band gap with composition is well described by the Zunger bowing model.

The Optical calculations demonstrate strong ultraviolet absorption and pronounced optical anisotropy, while the thermodynamic properties exhibit a significant dependence on temperature and pressure, indicating good thermal stability under varying operating conditions. Although the alloy compositions were modeled using ordered supercells, which do not explicitly account for configurational disorder, this approach successfully captures the essential composition-dependent trends. Overall, the present findings provide a comprehensive theoretical understanding of $AgAl(S_{1-x}Se_x)_2$ alloys and demonstrate their strong potential for ultraviolet optoelectronic applications, while offering a reliable foundation for future experimental studies and advanced device design.

## ORCID

**Nabil Beloufa,** https://orcid.org/0009-0007-5099-5180;
**Mohammed Ouled Ali,** https://orcid.org/0009-0006-3516-6328;
**Hamza Rekab-Djabri,** https://orcid.org/0000-0002-2458-1335;
**Djamel Eddine Belfennache,** https://orcid.org/0000-0002-4908-6058;
**Radhia Yekhlef,** https://orcid.org/0000-0003-0646-6453;
**Hamad M Adress Hasan,** https://orcid.org/0000-0002-6739-8311;
**Hanan F. Emrayed,** https://orcid.org/0009-0008-6812-4268;
**Ghada M Salem,** https://orcid.org/0000-0002-1830-7049

## REFERENCES

[1] F. Saker, L. Remache, D. Belfennache, K.R. Chebouki, and R. Yekhlef, Chalcogenide Lett. **22(2)**, 151 (2025). https://doi.org/10.15251/CL.2025.222.151
[2] R. Ouldamer, D. Madi, and D. Belfennache, in: *Advanced Computational Techniques for Renewable Energy Systems. IC-AIRES 2022. Lecture Notes in Networks and Systems*, vol. 591, edited by M. Hatti, (Springer, Cham. 2023). pp. 700-705, https://doi.org/10.1007/978-3-031-21216-1_71
[3] S. Mahdid, D. Belfennache, D. Madi, M. Samah, R. Yekhlef, and Y. Benkrima, J. Ovonic. Res. **19(5)**, 535-545 (2023). https://doi.org/10.15251/JOR.2023.195.535
[4] Y. Bellal, A. Bouhank, D. Belfennache, R. Yekhlef, East Eur. J. Phys. (1), 170 (2025). https://doi.org/10.26565/2312-4334-2025-1-16
[5] K. Bouferrache, M.A. Ghebouli, B. Ghebouli, M. Fatmi, S. Alomairy, T.M. Althagafi, N. Bioud, *et al*., Eur. Phys. J. Appl. Phys. **100**, 29 (2025). https://doi.org/10.1051/epjap/2025027
[6] A. Djemli, M. Reffas, K. Bouferrache, F. Benlakhdar, R. Yekhlef, D. Belfennache, and S.I. Ahmed, *et al*., Phys. Solid State, **67**(5), 356 (2025). https://doi.org/10.1134/S1063783425600499
[7] R.P. Brian, T. Kiyosawa, and K. Masumoto, Prog. Cryst. Growth Charact. **1**, 331 (1979). https://doi.org/10.1016/0146-3535(79)90002-9
[8] S. Prasad, and B.D. Pandey, Miner. Eng. **11**, 763 (1998). https://doi.org/10.1016/S0892-6875(98)00061-2
[9] H. Horinaka, S. Mononobe, and N. Yamamoto, Jpn. J. Appl. Phys. **32**, 109 (1993). https://doi.org/10.7567/JJAPS.32S3.109
[10] J. L. Shay, L. M. Schiavone, E. Buehler, and J. H. Wernick, J. Appl. Phys. **43,** 2805 (1972). https://doi.org/10.1063/1.1661599
[11] N. Uchitomi, and H. Kizaki, J. Magn. Magn. Mater. **597**, 172019 (2024) https://doi.org/10.1016/j.jmmm.2024.172019
[12] L.I. Koroleva, D.M. Zashchirinskii, T.M. Khapaeva, S.F. Marenkin, I.V. Fedorchenko, R. Szymczak, B. Krzumanska, *et al*., Phys. Solid State **51**, 303 (2009). https://doi.org/10.1134/S1063783409020164
[13] D. Belfennache, N. Brihi, and D. Madi, Proceeding of the IEEE xplore, 8th (ICMIC) (2016), pp. 497–502 (2017). https://doi.org/10.1109/ICMIC.2016.7804164
[14] K. Madoui, A Ghechi, S. Madoui, R. Yekhlef, D. Belfennache, S. Zaiou, and M.A. Ali, East Eur. J. Phys. (3), 390 (2024). https://doi.org/10.26565/2312-4334-2024-3-48
[15] O. Madkhali, Phys. Scr. **99**, 022004 (2024). https://doi.org/10.1088/1402-4896/ad1e44
[16] J. Low, J. Yu, M. Jaroniec, S. Wageh, A. Ahmed, A. Ghamdi, Adv. Mater. **29**, 1601694 (2017). https://doi.org/10.1002/adma.201601694
[17] J.Y. Tsao, S. Chowdhury, M.A. Hollis, D. Jena, N.M. Johnson, K.A. Jones, R.J. Kaplar, *et al*., Adv. Electron. Mater. **4**, 1600501 (2017). https://doi.org/10.1002/aelm.201600501.
[18] J.F. Randall, and J. Jacot, Renew. Energy, **28**, 1851 (2003). https://doi.org/10.1016/S0960-1481(03)00068-5
[19] J. E. Jaffe, and A. Zunger, Phys. Rev. B, **28**, 5822 (1983). https://doi.org/10.1103/PhysRevB.28.5822
[20] M.Ya. Rudysh, P.A. Shchepanskyi, G.L. Myronchuk, M. Piasecki, and O.S. Martyniuk, Physica B, **654**, 414731 (2023). https://doi.org/10.1016/j.physb.2023.414731
[21] S. Ullah, H.U. Din, G. Murtaza, T. Ouahrani, R. Khenata, and S.B. Omran, J. Alloys Compd. **617**, 575 (2014). https://doi.org/10.1016/j.jallcom.2014.08.058
[22] S. Kang, J. Wang, L. Yang, and S. W. Fan, Phys. Scr. **99**, 035923 (2024). https://doi.org/10.1088/1402-4896/ad23ac
[23] S. Mishra, and B. Ganguli, Solid State Commun. **151**, 523 (2011). https://doi.org/10.1016/j.ssc.2011.01.024
[24] H. Hahn, G. Frank, W. Klingler, A.D. Meyer, and G. Störger, Z. Anorg. Allg. Chem. **271**, 153 (1953). https://doi.org/10.1002/zaac.19532710307

[25] M. Yuan, D.B. Mitzi, O. Gunawan, A.J. Kellock, S.J. Chey, and V.R. Deline, Thin Solid Films, **519**, 852 (2010). https://doi.org/10.1016/j.tsf.2010.08.135
[26] M.Y. Rudysh, A.O. Fedorchuk, M.G. Brik, J. Grechenkov, D. Bocharov, S. Piskunov, A.I. Popov, and M. Piasecki, Materials, **16**, 7017 (2023). https://doi.org/10.3390/ma16217017
[27] W.N. Honeyman, and K.H. Wilkinson, J. Phys. D: Appl. Phys. **4**, 1182 (1971). https://doi.org/10.1088/0022-3727/4/8/319
[28] G.M.D. Nguimdo, E. Igumbor, S. Zambou, and D.P. Joubert, Comput. Condens. Matter. **21**, e00391 (2019). https://doi.org/10.1016/j.cocom.2019.e00391
[29] G.M.D. Nguimdo, and D.P. Joubert, Eur. Phys. J. B **88**, 113 (2015). https://doi.org/10.1140/epjb/e2015-50478-x
[30] P. Cheng, and Y. Yang, Acc. Chem. Res. **53**, 1218 (2020). https://doi.org/10.1021/acs.accounts.0c00157
[31] S. Agarwal, K. Weideman, D. Rokke, K.C. Vincent, D. Zemlyanov, and R. Agrawal, J. Mater. Chem. C, **12**, 325 (2024). https://doi.org/10.1039/D3TC03540A
[32] R.W. Robinson, Y. Han, H. Zhang, T. Ablekim, I. Khan, K.A. Persson, and A. Zakutayev, Chem. Rev. **120**, 4007 (2020). https://doi.org/10.1021/acs.chemrev.9b00600
[33] J. Wu, W. Huang, H. Liu, Z. He, B. Chen, S. Zhu, B. Zhao, Y. Lei, and X. Zhou, Cryst. Growth Des. **20**, 3140 (2020). https://doi.org/10.1021/acs.cgd.0c00018
[34] J. Yang, Q. Fan, Y. Yu, and W. Zhang, Materials **11**, 2370 (2018). https://doi.org/10.3390/ma11122370
[35] P. Blaha, K. Schwarz, G.K.H. Madsen, D. Kvasnicka, and J. Luitz, WIEN2k, An Augmented Plane Wave Plus Local Orbitals Program for Calculating Crystal Properties (Vienna, 2008).
[36] Y. Benkrima, D. Belfennache, R. Yekhlef, and A.M. Ghaleb, Chalcogenide Lett. **20**, 609-618 (2023). https://doi.org/10.15251/CL.2023.208.609
[37] K. Schwarz, P. Blaha, Comput. Mater. Sci. 28, 259 (2003). https://doi.org/10.1016/S0927-0256(03)00112-5
[38] Y. Achour, Y. Benkrima, I.Lefkaier, and D. Belfennache, J. Nano- Electron. Phys. **15**(1), 01018(5pp) (2023). https://doi.org/10.21272/jnep.15(1).01018
[39] Y. Benkrima, D. Belfennache, R. Yekhlef, M.E. Soudani, A. Souiga, and Y. Achour, East Eur. J. Phys. (2), 150 (2023). https://doi.org/10.26565/2312-4334-2023-2-14
[40] Y. Benkrima, S. Benhamida, and D. Belfennache, Dig. J. Nanomater. Bios. **18**(1), 11 (2023). https://doi.org/10.15251/DJNB.2023.181.11
[41] Y. Benkrima, M.E. Soudani, D. Belfennache, H. Bouguettaia, and A. Souigat, J. Ovonic. Res. **18(6),** 797 (2022). https://doi.org/10.15251/JOR.2022.186.797
[42] H. Rekab-Djabri, S. Zaiou, A. Azzouz-Rached, A. Benamrani, S. Daoud, D. Belfennache, R. Yekhlef, and N. Beloufa, East Eur. J. Phys. **3**, 298 (2025), https://doi.org/10.26565/2312-4334-2025-3-27
[43] D. Koller, F. Tran, and P. Blaha, Phys. Rev. B, **85**, 155109 (2012). https://doi.org/10.1103/PhysRevB.85.155109
[44] K. Choudhary, and F. Tavazza, Comput. Mater. Sci. **161**, 300 (2019). https://doi.org/10.1016/j.commatsci.2019.02.006
[45] A.H. Reshak, Physica B: Condens. Matter **369**, 243 (2005). https://doi.org/10.1016/j.physb.2005.08.038
[46] S.P. Bremner, M.Y. Levy, and C.B. Honsberg, Prog. Photovolt: Res. Appl. **16**, 225 (2008). https://doi.org/10.1002/pip.799
[47] W.N. Honeyman, and K.H. Wilkinson, J. Phys. D: Appl. Phys. **4**, 1182 (1971). https://doi.org/10.1088/0022-3727/4/8/319
[48] L. Vegard, Z. Phys. **5**, 17 (1921). https://doi.org/10.1007/BF01349680
[49] H. Harry, F. Günter, K. Wilhelm, and G.M. Anne, Z. Anorg. Allg. Chem. **271**, 153 (1953). https://doi.org/10.1002/zaac.19532710307
[50] C.H. Ho and C.C. Pan, AIP Adv. **2**, 022123 (2012). https://doi.org/10.1063/1.4718342
[51] M. Faizan, S. Li, Z. Liu, Z. Li, J. Xie, K. Zhou, Y. Fu, and L. Zhang, J. Mater. Chem. C **13**, 2853 (2025). https://doi.org/10.1039/D4TC04075A
[52] F.E.H. Hassan, H. Akbarzadeh, and M. Zoaeter, J. Phys.: Condens. Matter. **16**, 293 (2004). https://doi.org/10.1088/0953-8984/16/3/009
[53] J. Phillips, Rev. Mod. Phys. **42**, 317 (1970). https://doi.org/10.1103/RevModPhys.42.317
[54] J.E. Bernard, and A. Zunger, Phys. Rev. B, **34**, 5992(R) (1986). https://doi.org/10.1103/PhysRevB.34.5992
[55] M. Fox, Optical Properties of Solids, 2nd ed., Oxford University Press, Oxford, (2010).
[56] P.Y. Yu, and M. Cardona, Fundamentals of Semiconductors: Physics and Materials Properties, 4th ed., Springer, (2010). https://doi.org/10.1007/978-3-642-00710-1
[57] F. Wooten, *Optical Properties of Solids*, (Academic, 2016).
[58] D.R. Penn, Phys. Rev. **128**, 2093 (1962). https://doi.org/10.1103/PhysRev.128.2093
[59] G. Dresselhaus, A.F. Kip, and C. Kittel, Phys. Rev. **100**, 618 (1955). https://doi.org/10.1103/PhysRev.100.618
[60] L. Cavaleri, M. Papia, G. Macaluso, *et al*., Mater. Struct. **47**, 239 (2014). https://doi.org/10.1617/s11527-013-0058-9
[61] Ç. Yamçıçıer, S. Al, and C. Kürkçü, Physica B: Condens. Matter: 716, 417713 (2025). https://doi.org/10.1016/j.physb.2025.417713
[62] K. Randall, and A. Burnham, Propellants Explos. Pyrotech. **30**, 344 (2005). https://doi.org/10.1002/prep.200500024
[63] M. Blanco, A.M. Pendás, E. Francisco, J. Recio, and R. Franco, J. Mol. Struct.: THEOCHEM, **368**, 245 (1996). https://doi.org/10.1016/S0166-1280(96)90571-0
[64] M. Flórez, J. Recio, E. Francisco, M. Blanco, and A.M. Pendás, Phys. Rev. B, **66**, 144112 (2002). https://doi.org/10.1103/PhysRevB.66.144112
[65] E. Francisco, M. Blanco, and G. Sanjurjo, Phys. Rev. B, **63**, 094107 (2001). https://doi.org/10.1103/PhysRevB.63.094107
[66] H. Xiao, K.J. Tahir, and W.A. Goddard, J. Phys. Chem. Lett. **2**, 212 (2011). https://doi.org/10.1021/jz101565j
[67] A. Verma, and S. Bhardwaj, Phys. Scr. **79**, 015302 (2008). https://doi.org/10.1088/0031-8949/79/01/015302

# DFT АНАЛІЗ СТРУКТУРНИХ, ОПТОЕЛЕКТРОННИХ ТА ТЕРМОДИНАМІЧНИХ ХАРАКТЕРИСТИК ХАЛЬКОПІРИТУ $AgAl(S_{1-x}Se_x)_2$

**Набіль Белуфа[1,2], Мохаммед Улед Алі[2,3], Хамза Рекаб-Джабрі[2,4], Д. Белфеннаше[5], Р. Єхлеф[5], Хамад М. Адресс Хасан[6], Ханан Ф. Емрайєд[6], Ханібал Саїд Хатаб[7], Гада М. Салем[8]**

*[1]Гідрометеорологічний інститут навчання та досліджень IHFR, ІбнуРошд.Вр 7019, Оран, Алжир*
*[2]Лабораторія мікро- та нанофізики (LaMiN), Національна політехнічна школа Оран, ENPO-MA, BP 1523, Ель-М'Науер, 31000, Оран, Алжир*
*[3]Факультет наук про речовину, математики та комп'ютерних наук, Університет Ахмеда Драї, Адрар, Алжир*
*[4]Факультет наук про природу та життя та наук про Землю, Університет АкліМоханда-Ульхаджа, 10000, Буїра, Алжир*
*[5]Дослідницький центр промислових технологій CRTI, P.O. A/c 64, Черага, 16014 Алжир, Алжир*
*[6]Кафедра хімії, факультет природничих наук, Університет Омара аль-Мухтара, Лівія*
*[7]Факультет освіти, Аль-Мардж, Університет Бенгазі, Лівія*
*[8]Лівійське управління наукових досліджень, Триполі, Лівія*

У цій роботі ми досліджували структурні, оптоелектронні та термодинамічні властивості четвертинної сполуки $AgAl(S_xSe_{1-x})_2$. У цьому дослідженні використовувався метод FP-LAPW, реалізований у програмі Wien2k та інтегрований у структуру теорії функціоналу густини (DFT). Для обробки обмінного та кореляційного потенціалу використовується узагальнене градієнтне наближення (WC-GGA). Ми вивчали вплив складу на міцність утворення, видимий модуль пружності та об'єм кристалічної решітки. Згідно із зібраними даними, не спостерігається жодних відхилень у модулі стисливості порівняно із законом LCD, а також у постійній решітки порівняно із законом Вегарда. Підхід Цунгера та його колег було використано для визначення мікроскопічного джерела просторової кривизни. Порівняно з попередніми теоретичними дослідженнями, значення ширини забороненої зони, отримані з розрахунків зонної структури на основі модифікованого наближення потенціалу Бекке-Джонсона (mBJ), показують помітні покращення та набагато краще узгоджуються з експериментальними результатами для потрійних сполук. Оптичні властивості вказують на те, що статична діелектрична проникність $\varepsilon_1(0)$ зростає зі збільшенням концентрації x, тоді як енергія оптичної щілини одночасно зменшується; водночас діелектрична функція демонструє значну анізотропію в напрямку zz. Дослідження впливу теплової енергії на певні макроскопічні характеристики було проведено з використанням квазігармонічної моделі Дебая. Тим не менш, досліджені сплави показали стабільність при проміжних температурах від 0 до 800 K.

**Ключові слова:** *$AgAl(S_xSe_{1-x})_2$; FP-LAPW; WC-GGA; mBJ; закон Вегарда; квазігармоніка Дебая*